A Journal of the Gesellschaft Deutscher Chemiker

Angewandte International Edition GDCh Chemie

www.angewandte.org

Accepted Article

Title: Fine-Tuning of Chiral Microenvironments within Triple-Stranded Helicates for Enhanced Enantioselectivity

Authors: Jingjing Jiao, Jinqiao Dong, Yingguo Li, and Yong Cui

To be cited as: *Angew. Chem. Int. Ed.* 10.1002/anie.202104111

Link to VoR: https://doi.org/10.1002/anie.202104111

WILEY-VCH

10.1002/anie.202104111

RESEARCH ARTICLE

WILEY-VCH

Fine-Tuning of Chiral Microenvironments within Triple-Stranded Helicates for Enhanced Enantioselectivity

Jingjing Jiao[+[a,b]], Jinqiao Dong,[+[a]] Yingguo Li,[[a]] and Yong Cui*[[a]]

Abstract: *Here we report the formation of an unexpected and unique family of chiral helicates. Crystal structures show that these triple-stranded $Zn^{II}_2L_3$ complexes are held together by subcomponent assembly of axially chiral diamine-functionalized 1,1'-biphenol ditopic with 2-formylpyridine and Zn(II). Specifically, the molecular helicity of the complexes can be controlled by the absolute configurations of the bimetallic vertices, which has been shown to be homoconfiguration (ΔΔ) or mesomeric configuration (ΔΛ), depending critically on the bulky groups and length of the spacers. Fascinatingly, in this system we can engineer the space-restricted chiral microenvironments with varied polar and apolar moieties, which profoundly influence the binding affinities and chiral discrimination properties of the helicates, leading to highly enantio- and helix-sense-selective recognition for chiral amino alcohols (up to 9.35). This work reveals the transformation of single-molecule chirality to global supramolecular chirality within well-defined helicates and demonstrates their chiral discrimination are highly dependent on the superior microenvironments.*

Introduction

The helix is one of the most pervasive structural elements of biomolecules,[1] such as double-stranded DNA,[2] triple-stranded collagen,[3] and coiled-coil helix bundle proteins,[4] and is also the ubiquitous object in nature from microscopic to macroscopic points of view.[5] Most importantly, the specific twisting of the helical strands results in inherently chiral (that is, the right- and left-handed helices are exactly mirror images of each other).[6] Therefore, the constituent small molecules (e.g., nucleotides, carbohydrates, and amino acid) can form complex biomacromolecules with multi-level chiral characteristics[7] – the system generally contains multiple stereogenic centers. Such notable feature has led to fascinating chiral environments capable of exceptionally stereospecific interactions in biological systems by combining direct hydrogen-bonding with hydrophobic effect (see an example of avidin-biotin complex in Figure 1).[8] Inspired by nature, present-day researchers are actively pursuing the synthetic analogues. However, chemical knowledge of how to rationally designed artificial helices with outstanding enantioselective recognition has remained a mystery, presumably due to the intrinsic difficulties associated with the fine-tuning of chiral microenvironments for regulating enantiomer to helix interactions.[9]

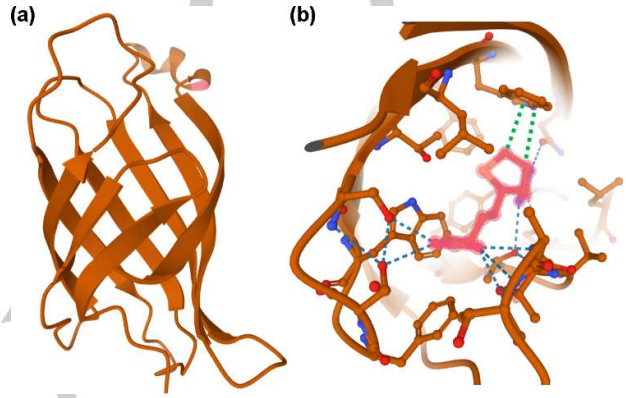

Figure 1. (a-b) An example of naturally chiral biomacromolecule with helical structure – eight-stranded avidin proteins are able to bind chiral biotin (avidin-biotin complex) with ultrahigh affinities and selectivities (up to 10^{15} M^{-1}) by combining hydrogen-bonding with hydrophobic effect (PDB: 2AVI).[8]

Helicates or metallohelices, pioneered by Lehn,[10] are discrete coordination complexes in which one or more organic ligands helically wrapped and coordinated to cations (or anions) by coordination bonds.[11] Typically, the assembly of pre-designed ligands and metal ions can form various helicates with structurally well-defined shapes and sizes, including double-stranded,[12] triple-stranded,[13] quadruple-stranded,[14] six-stranded,[15] and circular helicates.[16] For example, Nitschke and co-workers recently reported the assembly of six-stranded hollow helicates $[Ag^{I}_8L_6]$ and $[Ag^{I}_{12}L_6]$, where the templating anion plays an integral structure-defining role.[15b] More importantly, the length and flexibility of constitutive strands play a key factor for the helical conformation,[17] which is exemplified by the structural transformation between coordination cages and helicates. For instance, Clever and co-workers demonstrated that the helically twisted complex $[Pd^{II}_2L_4]$ can be generated by introducing isoquinoline donors.[14c] Interestingly, some of these structures are inherently chiral as a consequence of resulting *P*-configured and *M*-configured diastereomers.[12f, 12h, 14b, 18] However, they are depressed in chiral recognition, probably arising from the insufficient chiral microenvironments.[9, 19] Nevertheless, the use of enantiomerically pure ligands is able to drive the formation of chiral helicates that are capable of recognizing and converting substrates in their interior with enantioselective ways. We previously reported a quadruple-stranded helicate consisting of structurally flexible Salan-type ligands with central chirality,[14b] the resultant chiral microenvironment within the enclosed cavity has enabled the

[a] Dr. J. Jiao, Dr. J. Dong, Mr. L. Liu, Prof. Y. Cui
School of Chemistry and Chemical Technology, Frontiers Science Center for Transformative Molecules and State Key Laboratory of Metal Matrix Composites, Shanghai Jiao Tong University, Shanghai 200240, P. R. China
E-mail: yongcui@sjtu.edu.cn
[b] Dr. J. Jiao
The Key Laboratory of Resource Chemistry of Ministry of Education, Shanghai Key Laboratory of Rare Earth Functional Materials, Shanghai Normal University, Shanghai 200234, China
[+] These authors contributed equally to this work.

Supporting information for this article is given via a link at the end of the document.

chiral discriminations towards chiral amino acids. However, in this case the enantioselectivity is moderate (~3.69) owing to the difficulties in modifying the microenvironment within the nanocavity through installation of chiral binding sites and control of the hydrophobic effect. Thus, rationally designed well-defined helicates with exceptional chiral recognition performance remains a formidable challenge.

In this context, we develop a new system for self-assembly of well-defined chiral helicates from axially chiral 1,1′ -biphenyl-type ligands. X-ray crystal structures evidence that the absolute configurations of the bimetallic vertices of the helicates can adopt homoconfiguration (*ΔΔ*) or mesomeric configuration (*ΔΛ*), critically depending on the bulky groups and length of the spacers. Fascinatingly, the chiral microenvironments of the triple-stranded helicates involving molecular helicity, cavity sizes, chiral recognition sites, and hydrophobic surfaces can be finely tuned through the deployment of the pre-designed chiral ligands. It was found that the binding affinities and enantioselectivities of the helicates are significantly influenced by the hydrophobic effect and cavity sizes, leading to highly enantio- and helix-sense-selective recognition for a variety of chiral amino alcohols (up to 9.35), as unambiguously revealed by extensive experimental and theoretical results.

Results and Discussion

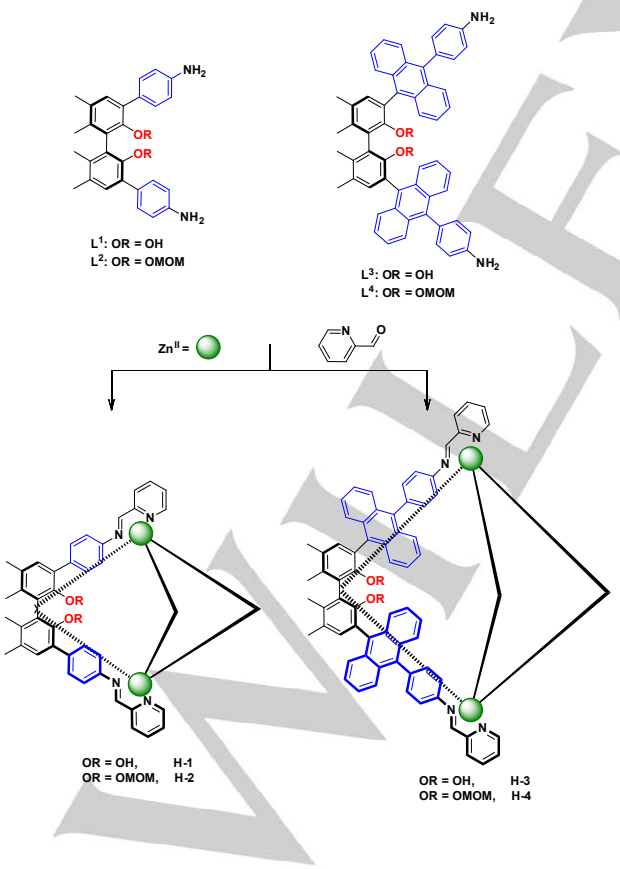

Scheme 1. Self-assembly of triple-stranded helicates **H-1-4** by using axially chiral 1,1′-biphenyl-type ligands.

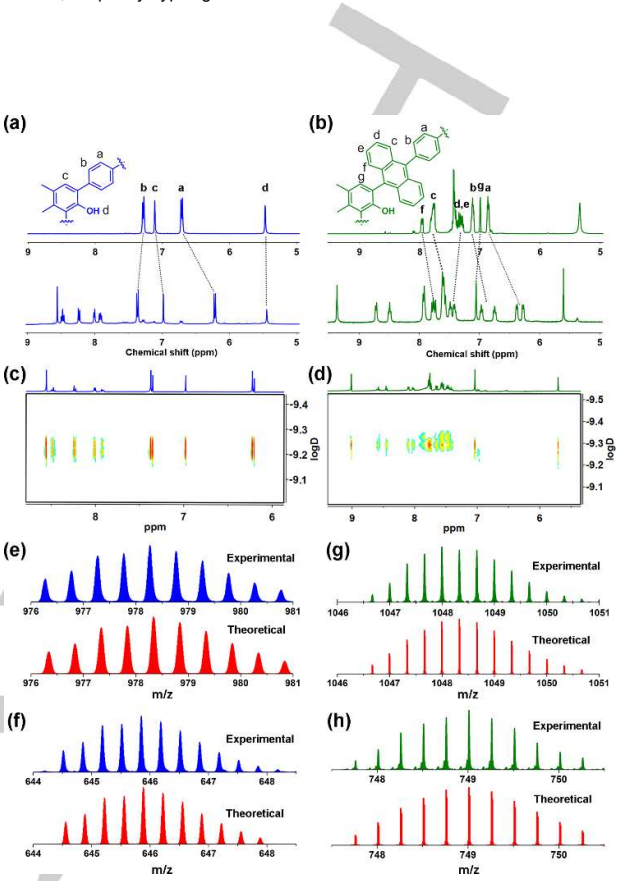

Figure 2. (a) Partial ^{1}H NMR spectra of **L^1** (up) and **H-1** (down). (b) Partial ^{1}H NMR spectra of **L^3** (up) and **H-3** (down). 2D DOSY spectra of **H-1** (c) and **H-3** (d). Experimental (Q-TOF-MS) and calculated isotope patterns of **H-1** (e, f), **H-3** (g, h).

Axially chiral molecules have been extensively used to develop optically functional materials with excellent enantioselective processes at the macroscopic scale, such as metal-organic frameworks (MOFs)[20] and covalent organic frameworks (COFs).[21] In particular, our previous work has shown a series of 1D helical coordination polymers that were formed by the assembly of chiral 1,1′-biphenyl-type ligands with C_2-symmetric coordinated Ag(I) ions.[22] In this study we employ such axially chiral ligands to construct discrete chiral helicates at the microscopic level. The enantiopure ligands **L^1**, **L^2**, **L^3** and **L^4** were prepared from (*R*)/(*S*)-appropriate diiodinated biphenol derivative through several steps with 42%, 40%, 15% and 12% overall yields, respectively. Full descriptions of the syntheses and characterizations for these ligands and intermediates are provided in Supporting Information (Figure S1-S15). Notably, it is impressive to observe that the chiral ligands are able to retain the high optical purity of the starting biphenol-type molecules after multi-step synthesis. For

example, the optical purity of **L**^{1} and **L**^{2} exceeds 95% enantiomeric excess (*ee*) value (Figure S16-S17), which is beneficial to assemble homochiral helicates with outstanding enantioselective recognition properties. As shown in Scheme 1, the reactions between ligand **L** (3 equiv.), 2-formylpyridine (6 equiv.), and $Zn(OTf)_2$ or $Zn(BF_4)_2$ (2 equiv.) in acetonitrile at 70 °C produce helicates **H-1**-**4** with general formula $[(Zn_2\mathbf{L}_3)A_4]\cdot G$ (**L** = **L**^{1}, **L**^{2}, **L**^{3} and **L**^{4}, A = counter anion, G = guest molecule) as the uniquely observed product. ^{1}H nucleus magnetic resonance (NMR) spectra of **H-1** displayed one set of ligand resonances (Figure 2a and Figure S18), suggesting the formation of discrete and highly symmetric metal-organic assemblies. Similarly, the ^{1}H NMR signals of **H-3** and **H-4** revealed that they have symmetric structures (Figure 2b and Figure S19-S22). While **H-2** showed two sets of equivalent ligand resonances (Figure S23-S24), meaning that the structure was distored which may arise from C_2 symmetry missing of biphenol in the helical complex. In all cases all of the proton signals are very sharp, implying the formation of discrete metal complexes rather than oligomeric species,[14b] as further confirmed via two-dimensional (2D) ^{1}H–^{1}H correlation spectroscopy (COSY) (Figure S27-S30) and ^{1}H–^{1}H nuclear Overhauser effect spectroscopy (NOESY) experiments (Figure S31-S34). Furthermore, ^{1}H NMR chemical shift on aromatic rings of ligands **L**^{1} ($H_{a,c}$) and **L**^{3} ($H_{a,b,c,g,f}$) appeared upfield attributed to the coordination with Zn^{2+} (Figure 2a,b). 2D Diffusion-ordered spectroscopy (DOSY) experiments also confirmed the formation of a single species with diffusion coefficients of 6.3×10^{-10}, 6.6×10^{-10}, 5.1×10^{-10}, and 4.0×10^{-10} m^2 s^{-1} for **H-1** to **H-4** (Figure 2c,d and Figure S35-S36), respectively. Dynamic diameters of these helicates determined by diffusion coefficients showed a increased size from **H-1** to **H-4**, which are in good agreements with their molecular structures.

The formation of triple-stranded helicates **H-1-4** was further identified by Quadrupole time-of-flight mass spectrometry (Q-TOF-MS), which are well consistent with the expected $Zn_2\mathbf{L}_3$ stoichiometry. Each spectrum exhibited a series of peaks with different charge states derived by the loss of anions (such as BF_4^- or OTf^-) or proton (Figure S37-S40). For **H-1**, the peaks at 675.18, and 978.28 Da can be assigned to $[Zn_2(\mathbf{L}^{1})_3(BF_4)]^{3+}$ and $[Zn_2(\mathbf{L}^{1})_3\text{-}2H\text{+}H_2O]^{2+}$, respectively. Furthermore, the experimental isotopic patterns of two or three charge states of **H-1** are in good agreement with the simulated isotopic distributions (Figure 2e,f). In the case of **H-3**, as expected, highly pure $Zn_2(\mathbf{L}^{3})_3$ supramolecular structure was also confirmed by the measured peaks of 1048.34 (simulated data at 1048.32 Da) and 749.01 Da (simulated data at 749.01 Da for $[Zn_2(\mathbf{L}^{3})_3(OTf)]^{3+}$ and $[Zn_2(\mathbf{L}^{3})_2]^{4+}$ (Figure 2g,h), respectively. As for **H-2** and **H-4**, clear assigned spectra were observed with peaks at 905.16, 784.21, and 553.79 Da for $[Zn_2(\mathbf{L}^{2})_2(OTf)_2]^{2+}$, $[Zn_2(\mathbf{L}^{2})_3(OTf)]^{3+}$, and $[Zn_2(\mathbf{L}^{2})_3\text{+}H_2O]^{4+}$, as well as 852.75 and 563.17 Da for $[Zn_2(\mathbf{L}^{4})_3\text{+}5CH_3CN]^{4+}$ and $[Zn_2(\mathbf{L}^{4})_2\text{+}2H_2O]^{4+}$ (Figure S38 and S40), respectively. Taken together, all the above Q-TOF-MS data indicate that the C_2-symmetric chiral ligands are preserved in the $Zn_2\mathbf{L}_3$ helicates with no existence of other isomers or conformers.

Single-crystal X-ray diffraction study on **H-1** evidenced the formation of helically triple-stranded complex. **H-1** crystallizes in the chiral trigonal *R*32 space group (Table S1-S2), with one third formula unit in the asymmetric unit (Figure 3a,b). The complex is composed of three **L**^{1} strands and two Zn^{2+}. The dinuclear Zn^{2+} locates on the vertices and three bis-bidentate ligands helically wrap and coordinate to it. Each metal center is approximately octahedral six-coordinated by bidentate chelating moieties with a mean average Zn–N bond length of 2.15 Å. The Zn-to-Zn distance is 13.7 Å and both metal centers are shown to be homoconfiguration (*ΔΔ*), thus resulting in homochiral characteristic that arises from facial (fac) stereochemistry (Figure 3c-d). By combining the chiral ligands, *P*-configured helical conformation, and the same handedness of metal centers, it has been suggested that **H-1** is capable of intriguing chiral characteristic that is expected to mimic natural biomacromolecule. Additionally, **H-1** has a nanosized cavity (12.5 Å × 4.8 Å × 4.8 Å) and entrance window (6.3 Å × 5.4 Å) occupied by guest molecules. Notably, the resultant microenviroment contains six hydroxyl groups that oriente toward inside of the pores accessible to guest molecules.

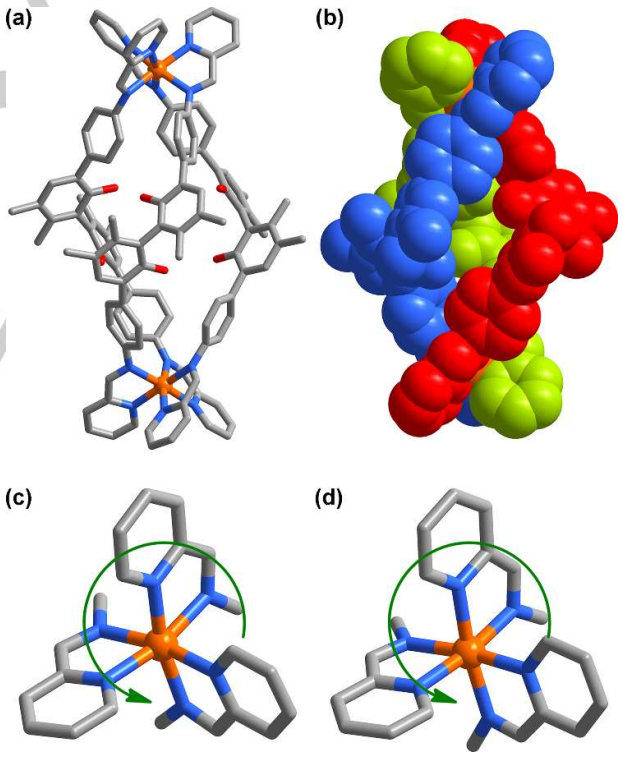

Figure 3. Single-crystal X-ray structure of ***ΔΔ*-H-1** (CCDC: 2047453) (a) and its space filling model (b). (c-d) The handedness of two Zn(II) centers shows homoconfiguration (*ΔΔ*).

Unfortunately, the weak X-ray diffraction limited the crystal structure determination in **H-2**. Instead, the high-quality single

crystal of **H-2 (Fe)** analogue was obtained, which has isomorphic structure with **H-2** as confirmed by ^{1}H and ^{13}C NMR (Figure S25-S26). Single-crystal X-ray diffraction data reveals that **H-2 (Fe)** crystallizes in the chiral orthorhombic $P2_12_12$ space group (Table S1 and S3), with one formula unit in the asymmetric unit (Figure 4a,b). As expected, **H-2 (Fe)** also showed a M_2L_3-type helical structure. However, it has to be mentioned that that the two Zn(II) centers displyed a mesomeric configuration (***ΔΛ***) (Figure 4c,d).[23] Such distinct handedness occurred in **H-2** or **H-2 (Fe)** may result from the relative steric hindrance of methoxymethoxy groups, and one of the three biphenol strands changes the twist direction to wrap around the metal centres. The reduced molecular helicity thus profoundly affects the chiral features of **H-2**. Additionally, strong intermolecular π−π and CH···π interactions direct the packing of the helicate **H-1** and **H-2 (Fe)** into porous 3D structures (Figure S41-S45).

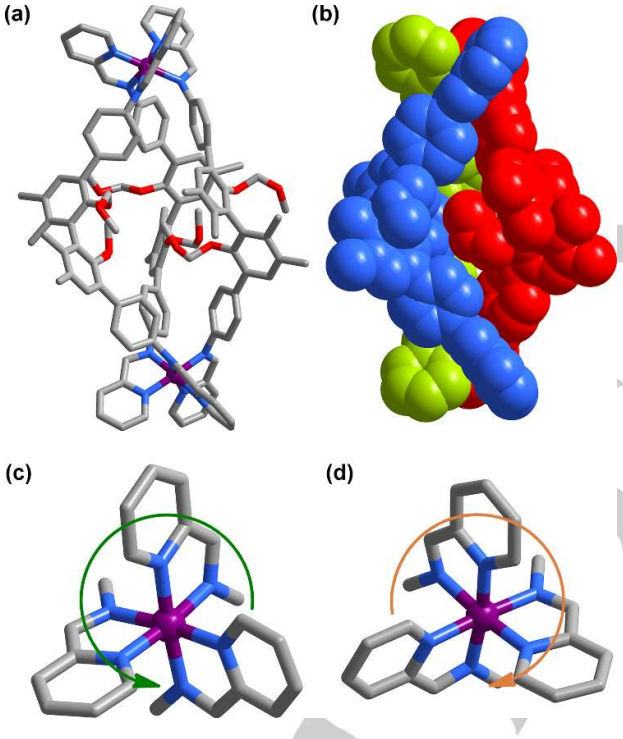

Figure 4. Single-crystal X-ray structure of ***ΔΛ*-H-2 (Fe)** (CCDC: 2049627) (a) and its space filling model (b). (c-d) The handedness of two Zn(II) centers shows mesomeric configuration (***ΔΛ***).

Numerous tries to achieve high-quality single crystals of **H-3** and **H-4** are unsuccessful. We thus performed molecular simulations to construct molecular models for **H-3** and **H-4** by DFT calculations (Figure 5). Owing to the decrease of steric hindrance within the nanocavity, the energy-minimized structures showed that the two Zn(II) centers adopt the same handedness with ***ΔΔ*** or ***ΛΛ*** configurations within **H-3** and **H-4**. The lengthened ligands $\mathbf{L^3}$ and $\mathbf{L^4}$ thus allow the formation of hollow helicates with more flexible strands, wider windows, and larger cavities relative to **H-1**/**H-2**. For example, the distance of Zn-to-Zn in **H-3** is 21.4 Å and cavity size is 19.4 Å × 6.2 Å × 6.2 Å. Impressively, by virtue of anthracene surfaces, the chiral microenvironment within **H-3** is capable of strong hydrophobic effect that can provide multiple hydrophobic/CH−π interactions for enhanced binding affinities and chiral discrimination properties. To the best of our knowledge, **H-3** represents a rare example of chiral helicates with rich chiral binding sites (polar moiety) and high-density hydrophobic walls (apolar moiety).

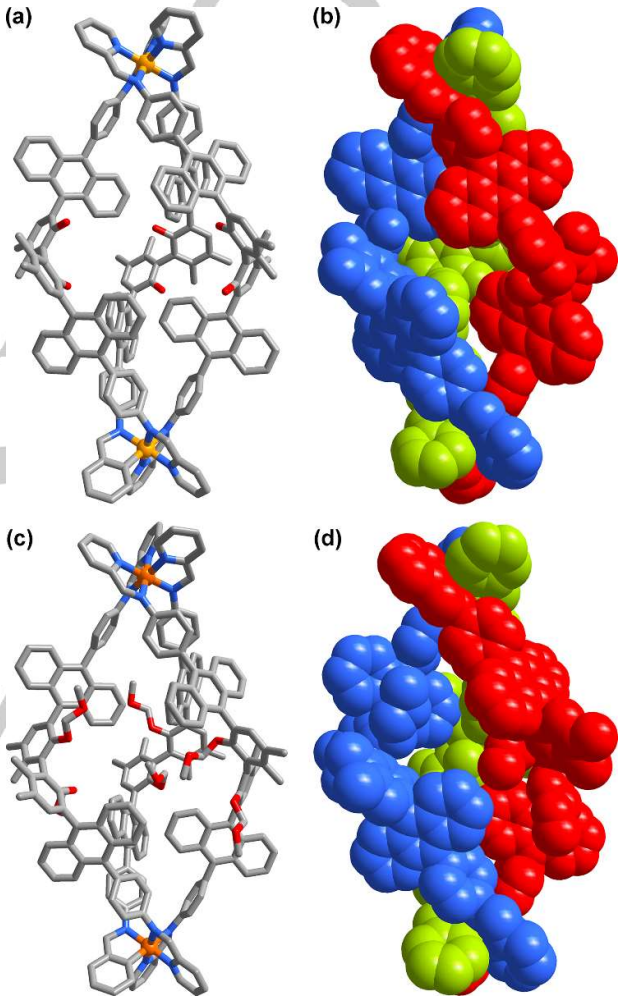

Figure 5. Energy-minimized molecular structures of ***ΔΔ*-H-3** (a) and ***ΔΔ*-H-4** (c), and their space filling models ***ΔΔ*-H-3** (b) and ***ΔΔ*-H-4** (d) based on DFT calculations.

The CD spectra of the four helicates made from (*R*)- and (*S*)-enantiomers are mirror images of each other indicative of their enantiomeric nature (Figure S46-S49). Surprisingly, the self-assembled helicates accompany chiral amplification effects. Firstly, Kuhn's dissymmetry factors (g_{abs}) can be employed to evaluate the chiral amplification behaviour.[24] In terms of UV-vis absorption and CD spectra

of helicates **H-1-4** and ligands $\mathbf{L^{1-4}}$, the obtained g_{abs} values of **H-1** (11.0×10^{-3}), **H-3** (6.3×10^{-3}), and **H-4** (3.5×10^{-3}) are higher than their corresponding ligands $\mathbf{L^1}$ (1.8×10^{-3}), $\mathbf{L^3}$ (0.1×10^{-3}) and $\mathbf{L^4}$ (1.5×10^{-3}) (Table S4), respectively, thus indicating the chiral transfer and amplification in the assembly process. However, the g_{abs} value of **H-2** (5.1×10^{-3}) exhibit smaller than $\mathbf{L^2}$ (9.4×10^{-3}), which may be attributed to the reduction of molecular helicity through its mesomeric configuration (*ΔΛ*). Secondly, the values of molar optical rotation (ϕ) of ***ΔΔ*-H-1** and (*R*)-$\mathbf{L^1}$ are 8832.5 and 970.1 deg·cm^3·dm^{-1}·mol^{-1}, respectively. The helicate bearing three ligands has an optical rotation per mole that is >9 times that of (*R*)-$\mathbf{L^1}$, meaning a 3-fold increase in optical rotation between a set of three free ligands and a set of three coordinated ligands. This implies that such helical-shaped suprastructure can indeed generate unexpectedly strong chirality amplification, which is expected to exhibit exceptional chiral recognition ability. Similar chiral amplifications were also observed for the other three helicates (Table S5). Other information such as Thermogravimetric analyses (TGA), Scanning electron microscopy (SEM), and Brunauer−Emmett−Teller (BET) surface areas are shown in the Supporting Information (Figure S50-S59).

Chiral 1,2-amino alcohols are imporant compounds due to their versatility as building blocks in the synthesis of natural products and commercial drugs.[25] The chiral discrimination of enantiomers of amino alcohols are therefore significant in the fields of medicinal and biological chemistry. ^{19}F NMR spectra showed only one kind of chemical environment of fluorine atom in all complexes (Figure S60-S63). By combining the crystal structures of ***ΔΔ*-H-1** and ***ΔΛ*-H-2 (Fe)** (Figure S42 and S45), it has been suggested that the identified counterions reside outside the cavities of the helicates. Fascinatingly, **H-1** and **H-3** containing the available recognition sites provide a good opportunity to realize the enantioselective recognition of chiral 1,2-amino alcohols. When **H-1** and **H-3** was treated with *D*-leucinol or *D*-valinol, the UV−vis spectrum remained unchanged, indicative of the stability of the host structure (Figure S64-S65).[26] In contrast to the absorption spectrum, however, the emission was changed. For instance, the fluorescence intensity of ***ΔΔ*-H-1** was enhanced by both *D*- and *L*-leucinol (**G1**), while the increase caused by *D*-leucinol was greater than *L*-leucinol (Figure S66). Furthermore, the Job plot result obtained by fluorescence titration suggested the formation of a 1:1 host-guest complex in this system (Figure S67). Figure 6b-c showed Benesi−Hildebrand plots with 1:1 binding model for ***ΔΔ*-H-1** in the presence of *D*- and *L*-leucinol in CH_3CN. The association constants K_a were found to be 4201 M^{-1} with *D*-leucinol and 1059 M^{-1} with *L*-leucinol, thus giving an enantioselectivity factor (EF) K_a(***ΔΔ*-*D*)/K_a(***ΔΔ*-*L*)** of 3.97 ± 0.04. Furthermore, the opposite trend in enantioselectivity was observed for the enhancement ***ΛΛ*-H-1** by leucinol, for which the EF [K_a(*ΛΛ*−*L*)/K_a(*ΛΛ*−*D*)] was 4.10 ± 0.06 (Figure 6c and Figure S68), further confirming a chirality-based luminescence-enhancing selectivity. Additionally, the 1:1 binding stoichiometry can be further confirmed by ESI-MS, which was performed at the identical concentration with fluorescence titration (Figure S69). The peaks at 603.27 and 869.59 are assigned to $[Zn_2(\mathbf{L^1})_3$+*D*-leucinol$]^{4+}$ and $[Zn_2(\mathbf{L^1})_3(BF_4)$+$CH_3CN$+$H_2O$+*D*-leucinol$]^{3+}$, which is consistent with the 1:1 binding stoichiometry of fluorescence titration. Notably, control exeprments showed that the free ligand $\mathbf{L^1}$ and mesomeric *ΔΛ*-**H-2** displayed no obvious enantioselectivities (Figure S70-S71), unambiguously suggesting that the chiral microenvironments and naked hydroxyl binding sites are extremely crucial for stereoselective recognition.

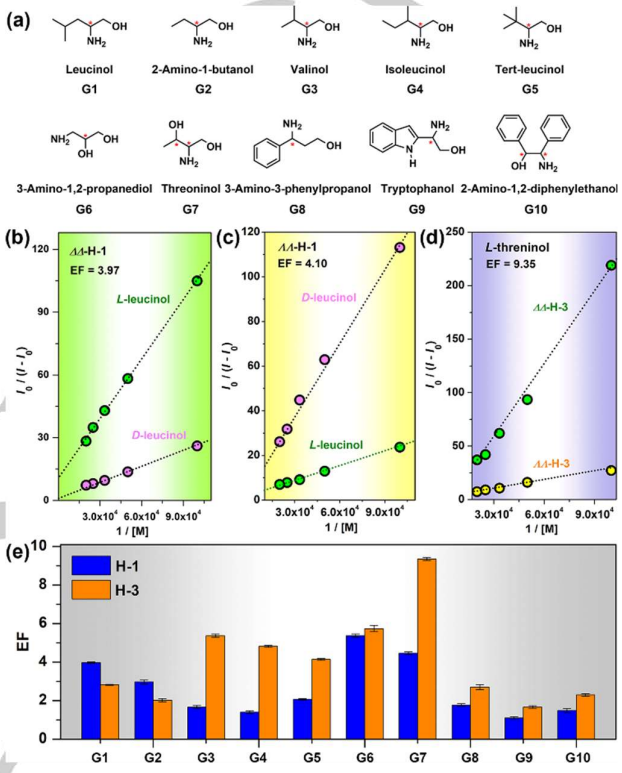

Figure 6. (a) Chemical structures of chiral amino alcohols used in this study. Benesi−Hildebrand plots of ***ΔΔ*-H-1** (b) and ***ΛΛ*-H-1** (c) titration with *D*- and *L*-leucinol. (c) Benesi−Hildebrand plots of ***ΔΔ*-H-3** and ***ΛΛ*-H-3** titration with *L*-threninol. (e) EF values of **H-1** and **H-3** for chiral amino alcohols. The concentration of helicates is 1.0×10^{-5} M in CH_3CN (3 mL) and the concentration of guests is 1.0×10^{-3} M in CH_3CN.

After titration with *D*-leucinol, the quantum yield of ***ΔΔ*-H-1** increased from 13.21% to 16.98% and the fluorescence lifetimes changed slightly from 3.46 ns to 3.56 ns (Figure S72-S73). suggesting that the enantioselective recognition might be a static enhancement process by the formation of a helicate−amino alcohol adduct by combining hydrogen-bonding with hydrophobic effects. To prove our hypotheses, we employed ^{1}H-^{1}H 2D NOESY and COSY to explore the host-guest binding (Figure S74-S75). As shown in Figure S75, the crossover signals at (5.52, 2.05 ppm) and (5.52, 4.19 ppm) in the 2D NOESY spectrum are assigned to the NH_2 group of *D*-leucinol with ***ΔΔ*-H-1**. Furthermore, ^{1}H NMR titration showed that the proton signals of ***ΔΔ*-H-1** became broad and have a slight downfield shift (Figure S76). These results indicate that the host-guest binding occurs in the cavity of the helicate.

Impressively, we found that the chiral microenvironments of the helicates involving cavity sizes, chiral binding sites, and hydrophobic effect significantly influence the binding affinities and chiral discrimination properties. Particularly, **H-3** was found to have excellent binding affinities towards a varity of chiral aminol alcohols including both alkyl (**G1** to **G7**) and aryl (**G8** to **G10**) substrates. For most substrates, **H-3** showed higher K_a values than that of **H-1** (Figure S77-S96, Table S6). Such difference might be attributed to the strong hydrophobic effect provided by the anthracene surface. For example, K_a values for **H-1** and **H-3** upon the same enantiomer of the substrates showed distinct difference with 1528 M^{-1} and 10802 M^{-1} for valinol (**G3**), 909 M^{-1} and 4040 M^{-1} for threoninol (**G7**), 253 M^{-1} and 2816 M^{-1} for 3-amino-3-phenylpropanol (**G8**), and 420 M^{-1} and 4965 M^{-1} for tryptophanol (**G9**) (see Table S6), respectively, demonstrating the higher binding affinities of **H-3**.

As expected, **H-3** showed more prominent enantioselectivities than **H-1** as a result of the superior chiral microenvironments. For the alkyl substates **G1** to **G4**, **H-1** exhibited a decreased trend in enantioselectivities (3.97, 2.97, 1.67, and 1.40, respectively) with the increase of bulky resistance. While **H-3** showed an increased trend (2.82, 2.02, 5.37, and 4.82, respectively) due to its larger cavity, implying that the cavity size of the helicate is crucial for binding affinities and enantioselectivities. For the substates **G7** to **G10**, both **H-1** and **H-3** displayed decreased EF values (such as **H-3**: from 9.35, 2.70, 1.67, to 2.30, respectively), indicating the confined effects (see the molecular sizes of **G1-G10** in Figure S97). This phenomenon might be explained that (1) the steric hindrance of bulky aromatic groups probably impaired the chiral recognition ability, as well as (2) the strong π···π and CH···π hydrophobic interactions occupy the main host-guest interations that weaken the hydrogen bonding Interactions. To prove our hypothesis, we empolyed another type of chiral amino alcohols as substrates that contain three hydrogen bonding groups (see **G6** and **G7**). Obviously, the enantioselective performance of both **H-1** and **H-3** were the highest among all substrates, implying that the formations of more hydrogen bonds can greatly enhance the chiral recognition. Moreover, comparing enantioselectivities of **H-1** with **H-3** for **G6** and **G7**, the higher EF values for **H-3** further indicate that the hydrophobic effect played a vital role in binding affinities and chiral discrimination properties. To further reveal the importance of chiral binding sites within the microenviroments, we performed the control experiments using **H-4** containing OMOM (methoxymethyl ether) protecting groups (Figure S98-S99). As expected, the EF values of **H-4** titrated by *D*/*L*-leucinol and *D*/*L*-valinol are only 1.14 and 1.13, respectively, which are smaller than **H-3** (2.82 for *D*/*L*-leucinol and 5.37 for *D*/*L*-valinol, respectively), highlighing the chiral binding sites within the nanocavity profoundly influence the enantioselectivities of the helicates. Taken together, **H-3** possesses larger hollow cavity, rich chiral binding sites, and high-density hydrophobic surfaces, leading to an exceptional enantioselectivity of 9.35 for threoninol. Despite many cavity-containing chiral materials inlcusing MOFs, COFs, metallacages, and metallacycles for chiral recognition have been developed,[9] the present **H-3** has been shown to exhibit a superior enantio- and helix-sense-selective recognition. For example, the EF value of **H-3** for valinol are obviously larger than the best-demonstrated chiral MOF (5.37 *vs* 3.12).[27]

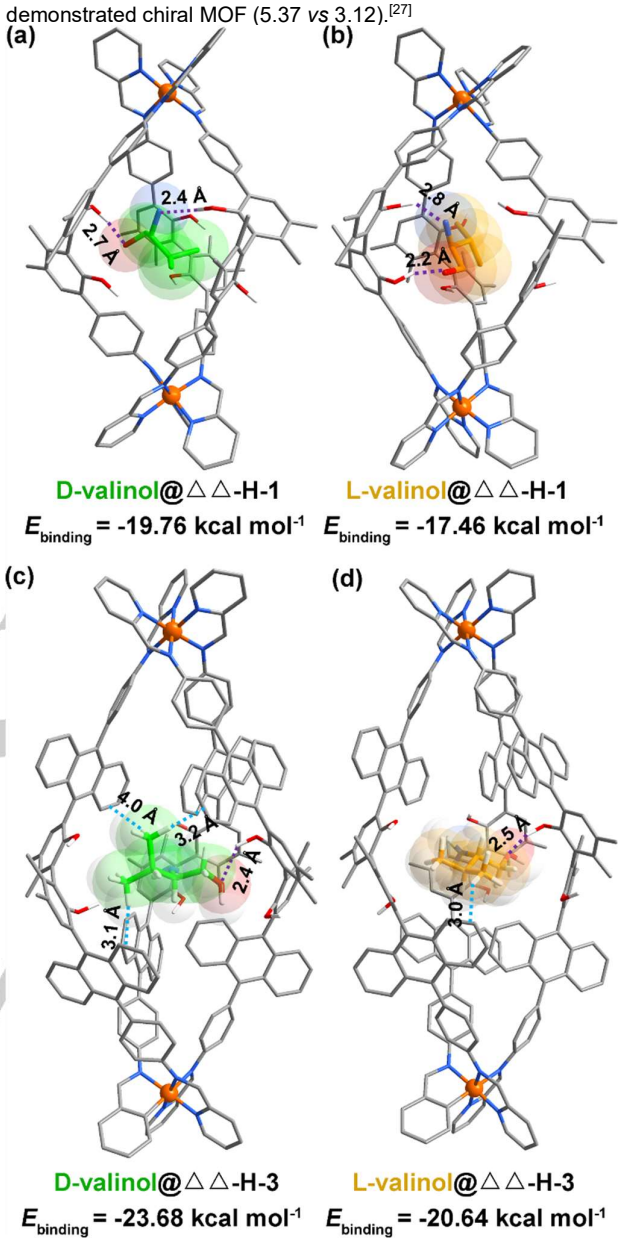

Figure 7. The host-guest conformation and binding energies of *D*-valinol@***ΔΔ*-H-1** (a), *L*-valinol@***ΔΔ*-H-1** (b), *D*-valinol@***ΔΔ*-H-3** (c), *L*-valinol@***ΔΔ*-H-3** (d) based on energy-minimized DFT calculations.

In an effort to understand the importance of the chiral microenviroments for enantioselective recognition, we thus carried out both experimental studies and theoretical calculations. On the one hand, it is interesting to note that very weak enantioselectivity (EF value of 1.51 ± 0.08) was observed for the luminescence enhancement of ***ΔΔ*-H-1** by *D*/*L*-*N*-Boc-protected leucinol (Figure S86), which implies the involvement of NH_2 groups in the formation of a ground-state hydrogen-bonded

complex. On the other hand, energy-minimized DFT calculations were performed to study the driving forces of host-guest binding within the chiral microenvironments of **H-1** and **H-3**.[28] We chose *D*/*L*-valinol as guests in terms of the greatest difference on EF values for **H-1** and **H-3** (1.67 *vs* 5.37). The conformation and binding energies of both enantiomers were evaluated by inserting ***ΔΔ*-H-1** and ***ΔΔ*-H-3** and performing energy minimization for the host−guest structures. As shown in Figure 7, the optimized structures showed that there have several host-guest interactions including hydrogen bonds (OH···N or OH···O) (2.2 ~ 2.8 Å) as well as π···π and CH···π interactions (3.0 ~ 4.0 Å). For the host-guest complexes *D*-valinol@***ΔΔ*-H-1**, *L*-valinol@***ΔΔ*-H-1**, *D*-valinol@***ΔΔ*-H-3**, and *L*-valinol@***ΔΔ*-H-3**, the binding energies were calculated to be -19.76, -17.46 -23.68 and -20.64 kcal mol^{-1}, respectively. The negative values of binding energies suggest that the hollow helicates are avaliable to encapsulate the enantiomers. Furthermore, the binding energies for *D*-valinol were more negative to that for *L*-valinol in both helicates, indicating a stronger host-guest interaction of ***ΔΔ*-H-1** and ***ΔΔ*-H-3** with *D*-valinol than *L*-valinol which result in enantioselective recognition. In particular, the anthracene groups within ***ΔΔ*-H-3** can provide more hydrophobic surface for binding guest molecules, thus giving rise to a stronger host-guest interaction (-23.68 vs -19.76 kcal mol$^{-1)}$ (Figure 7a and 7c). The theoretical calculations are well consistent with the experimental results, unambiguously revealing the critical importance of the chiral microenviroments for chiral recognition.

Conclusion

We have developed a new system for construction of structurally well-defined helicates with fine-tuning of chiral microenvironments. The use of axially chiral 1,1′-biphenyl-type ligands, Zn (II), and 2-formylpyridine to form a group of triple-stranded $Zn^{II}_2L_3$ helicates. These complexes are well characterized by Single-crystal X-ray diffraction, ^{1}H NMR, Q-TOF-MS, and CD spectra. Specifically, we find that the molecular helicity of the helicates can be tuned by the absolute configurations of the two metal centers with homoconfiguration (***ΔΔ***) or mesomeric configuration (***ΔΛ***), depending critically on the bulky groups and length of the spacers. Furthermore, the powerful coordination self-assembly allow us to finely tune the resulting chiral microenvironments of the helicates involving cavity sizes, chiral binding sites, and hydrophobic effect through the deployment of pre-designed chiral ligands. It has been suggested that such structural tunability can greatly enhance the host-guest binding affinities and chiral recognition ability. The present helicate **H-3**, which has suitable cavity size, rich chiral binding sites, and high-density hydrophobic surfaces, possesses exceptional enantioselectivities for a varity of chiral amino alcohols. This work thus reveals the chiral recognition performance of host materials are highly dependent on the subtly chiral microenvironments, which could facilitate the design of other cavity-containing chiral materials with outstanding enantioselective processes.

Acknowledgements

This work was financially supported by the National Science Foundation of China (Grant Nos. 91956124, 21875136, 21901164, 21620102001 and 91856204), the National KeyBasic Research Program of China (2016YFA0203400), Key Project of Basic Research of Shanghai (18JC1413200 and 19JC1412600), Shanghai Sailing Program (19YF1436100) and Shanghai Chenguang Project (18CG48).

Conflict of interest

The authors declare no conflict of interest.

Keywords: Helicates • Coordination complexes • Self-assembly • Chiral microenvironments • Enantioselective recognition

[1] a) E. Yashima, N. Ousaka, D. Taura, K. Shimomura, T. Ikai, K. Maeda, *Chem. Rev.* **2016**, *116*, 13752–13990; b) D. N. Woolfson, E. G. Baker, G. J. Bartlett, *Science* **2017**, *357*, 133–134.

[2] J. D. Watson, F. H. C. Crick, *Nature* **1953**, *171*, 737–738.

[3] D. R. Walker, S. A. H. Hulgan, C. M. Peterson, I. C. Li, K. J. Gonzalez, J. D. Hartgerink, *Nat. Chem.* **2021**, *13*, 260–269.

[4] A. R. Thomson, C. W. Wood, A. J. Burton, G. J. Bartlett, R. B. Sessions, R. L. Brady, D. N. Woolfson, *Science* **2014**, *346*, 485–488.

[5] X. Li, S. Chen, W.-D. Zhang, H. G. Hu, *Chem. Rev.* **2020**, *120*, 10079–10144.

[6] E. Yashima, K. Maeda, *Macromolecules* **2008**, *41*, 3–12.

[7] M. Frenkel-Pinter, M. Samanta, G. Ashkenasy, L. J. Leman, *Chem. Rev.* **2020**, *120*, 4707–4765.

[8] O. Livnah, E. A. Bayer, M. Wilchek, J. L. Sussman, *Proc. Natl. Acad. Sci. USA* **1993**, *90*, 5076–5080.

[9] J. Dong, Y. Liu, Y. Cui, *Acc. Chem. Res.* **2021**, *54*, 194–206.

[10] a) J. M. Lehn, A. Rigault, J. Siegel, J. Harrowfield, B. Chevrier, D. Moras, *Proc. Natl. Acad. Sci. USA* **1987**, *84*, 2565–2569; b) U. Koert, M. M. Harding, J.-M. Lehn, *Nature* **1990**, *346*, 339–342.

[11] C. Piguet, G. Bernardinelli, G. Hopfgartner, *Chem. Rev.* **1997**, *97*, 2005–2062.

[12] a) V. E. Campbell, X. de Hatten, N. Delsuc, B. Kauffmann, I. Huc, J. R. Nitschke, *Nat. Chem.* **2010**, *2*, 684–687; b) K. Miwa, Y. Furusho, E. Yashima, *Nat. Chem.* **2010**, *2*, 444–449; c) D. Zhao, T. van Leeuwen, J. Cheng, B. L. Feringa, *Nat. Chem.* **2017**, *9*, 250–256; d) J. F. Ayme, J. M. Lehn, C. Bailly, L. Karmazin, *J. Am. Chem. Soc.* **2020**, *142*, 5819–5824; e) N. Ousaka, M. Itakura, A. Nagasaka, M. Ito, T. Hattori, D. Taura, T. Ikai, E. Yashima, *J. Am. Chem. Soc.* **2021**, *143*, 4346–4358; f) J. L. Greenfield, E. W. Evans, D. Di Nuzzo, M. Di Antonio, R. H. Friend, J. R. Nitschke, *J. Am. Chem. Soc.* **2018**, *140*, 10344–10353; g) S. J. Allison, D. Cooke, F. S. Davidson, P. I. P. Elliott, R. A. Faulkner, H. B. S. Griffiths, O. J. Harper, O. Hussain, P. J. Owen-Lynch, R. M. Phillips, C. R. Rice, S. L. Shepherd, R. T. Wheelhouse, *Angew. Chem. Int. Ed.* **2018**, *57*, 9799–9804; *Angew.Chem.* **2018**, *130*, 9947–9952; h) Y. Suzuki, T. Nakamura, H. Iida, N. Ousaka, E. Yashima, *J. Am. Chem. Soc.* **2016**, *138*, 4852–4859.

[13] a) J. Hamacek, S. Blanc, M. Elhabiri, E. Leize, A. Van Dorsselaer, C. Piguet, A.-M. Albrecht-Gary, *J. Am. Chem. Soc.* **2003**, *125*, 1541–1550; b) L. Aboshyan-Sorgho, H. Nozary, A. Aebischer, J. C. G. Bünzli, P. Y. Morgantini, K. R. Kittilstved, A. Hauser, S. V. Eliseeva, S. Petoud, C. Piguet, *J. Am. Chem. Soc.* **2012**, *134*, 12675–12684; c) F. Li, J. K. Clegg, L. F. Lindoy, R. B.

Macquart, G. V. Meehan, *Nat. Commun.* **2011**, *2*, 205; d) C. Jia, W. Zuo, D. Yang, Y. Chen, L. Cao, R. Custelcean, J. Hostaš, P. Hobza, R. Glaser, Y. Y. Wang, X. J. Yang, B. Wu, *Nat. Commun.* **2017**, 8, 938; e) S. E. Howson, A. Bolhuis, V. Brabec, G. J. Clarkson, J. Malina, A. Rodger, P. Scott, *Nat. Chem.* **2012**, *4*, 31–36; f) A. D. Faulkner, R. A. Kaner, Q. M. A. Abdallah, G. Clarkson, D. J. Fox, P. Gurnani, S. E. Howson, R. M. Phillips, D. I. Roper, D. H. Simpson, P. Scott, *Nat. Chem.* **2014**, *6*, 797–803; g) C. J. Massena, N. B. Wageling, D. A. Decato, E. Martin Rodriguez, A. M. Rose, O. B. Berryman, *Angew. Chem. Int. Ed.* **2016**, *55*, 12398–12402; *Angew.Chem.* **2016**, *128*, 12586–12590; h) C. J. Massena, D. A. Decato, O. B. Berryman, *Angew. Chem. Int. Ed.* **2018**, *57*, 16109–16113; *Angew.Chem.* **2018**, *130*, 16341–16345; i) X. Chen, T. M. Gerger, C. Räuber, G. Raabe, C. Göb, I. M. Oppel, M. Albrecht, *Angew. Chem. Int. Ed.* **2018**, *57*, 11817–11820; *Angew.Chem.* **2018**, *130*, 11991–11994; j) X. Chen, C. Mevissen, S. Huda, C. Göb, I. M. Oppel, M. Albrecht, *Angew. Chem. Int. Ed.* **2019**, *58*, 12879–12882; *Angew.Chem.* **2019**, *131*, 13011–13014; k) X. Z. Li, L. P. Zhou, L. L. Yan, D. Q. Yuan, C. S. Lin, Q.-F. Sun, *J. Am. Chem. Soc.* **2017**, *139*, 8237–8244; l) L. Liang, B. Li, W. Zhang, A. Li, B. Zheng, X. J. Yang, B. Wu, *Angew. Chem. Int. Ed.* **2021**, *60*, 9389–9394; *Angew. Chem.* **2021**, *133*, 9475–9480; m) X. Li, J. Wu, L. Wang, C. He, L. Chen, Y. Jiao, C. Duan, *Angew. Chem. Int. Ed.* **2020**, *59*, 6420–6427; *Angew.Chem.* **2020**, *132*, 6482–6489.

[14] a) P. J. Steel, D. A. McMorran, *Chem. Asian J.* 2019, 14, 1098–1101; b) W. Xuan, M. Zhang, Y. Liu, Z. Chen, Y. Cui, *J. Am. Chem. Soc.* **2012**, *134*, 6904–6907; c) I. Regeni, B. Chen, M. Frank, A. Baksi, J. J. Holstein, G. H. Clever, *Angew. Chem. Int. Ed.* **2021**, *60*, 5673–5678; d) A. K. Mondal, H. S. Jena, A. Malviya, S. Konar, *Inorg. Chem.* **2016**, *55*, 5237–5244.

[15] a) M. Albrecht, K. Witt, H. Röttele, R. Fröhlich, *Chem. Commun.* **2001**, 1330–1331; b) C. T. McTernan, T. K. Ronson, J. R. Nitschke, *J. Am. Chem. Soc.* **2021**, *143*, 664–670.

[16] a) C. S. Wood, T. K. Ronson, A. M. Belenguer, J. J. Holstein, J. R. Nitschke, *Nat. Chem.* **2015**, *7*, 354–358; b) D. A. Leigh, R. G. Pritchard, A. J. Stephens, *Nat. Chem.* **2014**, *6*, 978–982; c) J. F. Ayme, J. E. Beves, C. J. Campbell, D. A. Leigh, *J. Am. Chem. Soc.* **2019**, *141*, 3605–3612; d) T. Y. Bing, T. Kawai, J. Yuasa, *J. Am. Chem. Soc.* **2018**, *140*, 3683–3689; e) Y. B. Tan, Y. Okayasu, S. Katao, Y. Nishikawa, F. Asanoma, M. Yamada, J. Yuasa, T. Kawai, *J. Am. Chem. Soc.* **2020**, *142*, 17653–17661.

[17] B. Li, W. Zhang, S. Lu, B. Zheng, D. Zhang, A. Li, X. Li, X.-J. Yang, B. Wu, *J. Am. Chem. Soc.* **2020**, *142*, 21160–21168.

[18] J. Gómez-González, Y. Pérez, G. Sciortino, L. Roldan-Martín, J. Martínez-Costas, J. D. Maréchal, I. Alfonso, M. Vázquez López, M. E. Vázquez, *Angew. Chem. Int. Ed.* **2021**, *60*, 8859–8866; *Angew. Chem.* **2021**, *133*, 8941–8948.

[19] L. J. Chen, H. B. Yang, M. Shionoya, *Chem. Soc. Rev.* **2017**, *46*, 2555–2576.

[20] a) H. Jiang, K. Yang, X. Zhao, W. Zhang, Y. Liu, J. Jiang, Y. Cui, *J. Am. Chem. Soc.* **2021**, *143*, 390–398; b) H. Jiang, W. Zhang, X. Kang, Z. Cao, X. Chen, Y. Liu, Y. Cui, *J. Am. Chem. Soc.* **2020**, *142*, 9642–9652.

[21] B. Hou, S. Yang, K. Yang, X. Han, X. Tang, Y. Liu, J. Jiang, Y. Cui, *Angew. Chem. Int. Ed.* **2021**, *60*, 6086–6093; *Angew. Chem.* **2021**, *133*, 6151–6158.

[22] Y. Liu, X. Xi, C. Ye, T. Gong, Z. Yang, Y. Cui, *Angew. Chem. Int. Ed.* **2014**, *53*, 13821–13825; *Angew. Chem.* **2014**, *50,* 14041–14045.

[23] a) M. Albrecht, S. Kotila, *Angew. Chem. Int. Ed.* **1995**, *34*, 2134–2137; *Angew. Chem.* **1995**, *107,* 2285–2287; b) M. Albrecht, C. Riether, *Chem. Ber. **1996***, *129*, 829–832.

[24] K. Terao, Y. Terao, A. Teramoto, N. Nakamura, M. Fujiki, T. Sato, *Macromolecules* **2001**, *34*, 6519–6525.

[25] D. J. Ager, I. Prakash, D. R. Schaad, *Chem. Rev.* **1996**, *96*, 835–876.

[26] J. Dong, C. Tan, K. Zhang, Y. Liu, P. J. Low, J. Jiang, Y. Cui, *J. Am. Chem. Soc.* **2017**, *139*, 1554–1564.

[27] M. M. Wanderley, C. Wang, C.-D. Wu, W. Lin, *J. Am. Chem. Soc.* **2012**, *134*, 9050–9053.

[28] J. Jiao, Z. Li, Z. Qiao, X. Li, Y. Liu, J. Dong, J. Jiang, Y. Cui, *Nat. Commun.* **2018**, *9*, 4423.

10.1002/anie.202104111

WILEY-VCH

Entry for the Table of Contents

We report the self-assembly of a new family of triple-stranded helicates with fascinating chiral characteristics from axially chiral 1,1′-biphenyl-type ligands. The fine-tuning of chiral microenvironments within the well-defined complexes has enabled outstanding chiral discrimination properties, leading to highly enantio- and helix-sense-selective recognition for chiral amino alcohols (up to 9.35).

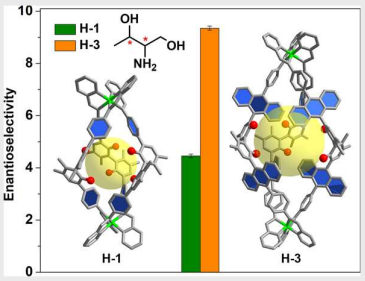

*Dr. Jingjing Jiao, Dr. Jinqiao Dong, Yingguo Li, and Prof. Yong Cui**

Page No. – Page No.

Fine-Tuning of Chiral Microenvironments within Triple-Stranded Helicates for Enhanced Enantioselectivity